On the potential of clustering approaches for hygrothermal material properties based on 3 degradation risks in solid masonry constructions

Bruno Vanderschelden, Klaas Calle, Nathan Van Den Bossche

Abstract

Historic masonry has a rich and colorful history making it a treasured part in our society. To preserve and protect this heritage, adequate moisture control, retrofit and restauration strategies are required. However, due to the large range of material properties inherent to historic brickwork, a single uniform renovation strategy appears impossible. To describe similarity in brickwork, the existing clustering approach developed by Zhao (2012) was evaluated. The idea is that different types of bricks with similar properties can be represented by a single representative brick for that cluster, e.g., when conducting hygrothermal simulations. It could help improve existing retrofit practice by reducing characterization processes and minimizing time-consuming measuring tests. However, in this paper the approach presented by Zhao is questioned since the clustering is solely based on an equal impact of the material properties and the response behavior and associated degradation risks are neglected. The aim of this paper twofold. Firstly, similarity in brickwork obtained by clustering according to Zhao was evaluated by means of hygrothermal simulations to see whether bricks in the same cluster show similar degradation risks. Zhao's clustering provides homogenous clusters regarding physical material properties, but significant variation was found in degradation risks for different bricks within the same cluster. Secondly, a methodology is presented to translate similarities in degradation profiles towards similarities in material properties. Sensitivity analyses were used to study the response behavior based on three degradations risks: mould growth, wood rot and frost damage. Finally, an overall clustering scheme was generated for brickwork, based on classification trees for different degradation phenomena.

Keywords

Numerical HAM simulation, Clustering analysis, Sensitivity analysis, Masonry degradation, Historic masonry renovation

Introduction

Brickwork is abundantly scattered throughout Europe and the historic masonry façade is highly profiled, rendering it an indispensable part of our society. Protecting these treasures from the changing climate and harsh weathering conditions is becoming a complex task, pushing the topic forward within the building physics research field (Leisnner and Killian, 2014; Mosoarca et al, 2018; Vandemeulebroucke et al, 2019, 2021; Viles, 2002, Zhou et al, 2020). Historic brickwork in our patrimonial experienced a complex and extensive history (Calle, 2020; Campbell, 2016; Le Noir, 2017; Peirs, 1979, 2005; Rothea and Hoffman, 1956; Stenvert, 2007,2012). It was first brought to the Northern and Middle parts of Europe during roman times. In the medieval era, when flammable building materials were prohibited after the great fires, brickwork became more prominent in the city centers and the countryside was quickly followed as well. However, the greatest impact within brick history came with the industrial revolution when the production of bricks became a mechanical process. Its dynamic history together with large variation in raw material, drying and baking processes resulted in a complex material with large variability (Le Noir, 2017). This wide variety is evident in the different colors and physical characteristics of the material. Unfortunately, this complicates the identification process of bricks in renovation projects today (Calle, 2020; Zhao, 2012). Renovation studies focusing historic masonry require the thermal as well as the hygric material properties to enable a reliable risk assessment. The determination of these properties can be done by a series of extensive laboratory tests, such as mercury intrusion, pressure plate, sorption isotherm tests etc. (Zhao, 2012). Note that a complete characterization of a material is very complex, costly, and takes several months. Especially the vapor and liquid transfer properties, as well as the storage at high moisture contents can be challenging to measure accurately. Therefore, a stochastic simulation approach was proposed in which numerical simulations are performed with sampling based on stochastics and correlations between material properties (Calle, 2020). Both strategies require either a lot of testing or computational time to derive a complete and reliable risk assessment. Therefore, Zhao proposed to use a clustering analysis which can create homogeneous brick clusters based on the similarity of their physical properties. In that process, a generic material is created through averaging, and that material should be representative for all elements within its cluster. This approach dramatically reduces the measuring and/or computational time for brick properties and provides great added value to renovation as well as new construction projects. The original clustering analysis done by Zhao focused on 23 brick types, but might potentially be applied to other material groups, e.g., mortars, natural stones, wood, and bio-based building materials. However, some assumptions of Zhao can be questioned. Only physical characteristics were considered as clustering variables and an equal weight was adopted for the different properties. In his analysis, the response behavior of materials was neglected, and hence the sensitivity for degradation was not considered. This paper presents an approach to push the scope of cluster analysis by including the response behavior.

Methods

This study was divided according to a threefold approach. In the first part, Zhao's clustering method was evaluated because of the equal weight of clustering variables as well as the absence of a response behavior for degradations. Heat Air Moisture (HAM) simulation were used to test the robustness to predict similar response behavior within one cluster, based on three state-of-the art numerical degradation models. As will be discussed in the next sections, this analysis showed that similar material properties were not a guarantee for a reliable similarity amongst degradation profiles. Therefore, in a second part the scope was pushed and the relation between the response behavior and physical properties was assessed based on various sensitivity analyses. This included scatterplots, binary Poison distribution-based classification trees as well as Spearman rank correlations (Calle, 2020, 2021; Hambdy, 1994; Hagentoft, 2013). Three numerical degradation models were adopted and because of their inherent differences in nature, the results were first analyzed separately. In the final part of the study, a single decision tree was created to put materials in different clusters based on the results of part two. The decision trees were created as they provide the reader with a prompt and comprehensive statistical analysis of classification. The individual degradation results were summarized in an overall flow chart combining the physical characteristics as well as the response behavior of the various brick types.

Clustering analysis based on physical properties

In the first part, the clustering analysis approach of Zhao (2012) was performed with the R-software accompanied with a validation process in the statistical program Spss (Statistical Package for the Social Science) [IBM SPSS Statistics 26 Documentation]. Clusters were created based on the physical properties and describes the similarities of materials by means of the distance between material properties (Everit, 1987, 2011; Zhao, 2012). An overview of different clustering methods: single, average, complete linkage as well as the Ward's method is given by Zhao (2012). He chose the Ward's method as it showed to be the most robust manner of clustering with a good handling of outliers in the dataset. The method consists of the fusion of individuals based on the smallest distance between centroids. Different calculation methods for the distance can be considered. In this research paper as well as in the research by Calle (2020) and Zhao (2012), the Euclidean distance based on the Pythagorean formulation was used. The centroid, in turn, is determined by the average of the individuals which have already been appointed to the cluster. According to Zhao, the following material properties are to be considered for

clustering: open porosity, effective saturation moisture content, capillary moisture content, moisture content measured at logarithmic capillary pressure (pC) 4.78 and 5.60, moisture content measured at 80% relative humidity, water vapor diffusion resistance factor, water absorption coefficient, thermal conductivity, and specific heat capacity. Remaining material properties were excluded due to a high correlation with others. To start, the material characteristics were normalized to a unit variance to omit the impact of absolute values. Zhao decided to create four clusters to represent the complete variety of bricks. Cluster 1 contains the modern bricks manufactured with new technology. Cluster 2 includes historical bricks fabricated with the classic loam and clay. Cluster 3 is composed of the historical bricks produced by clay, loam, and sand components. Cluster 4 has the bricks exhibiting higher density and lower liquid water transport abilities compared to the rest. Subsequently, four different generic materials were calculated by averaging the properties and material functions i.e., moisture retention curve (MRC) and liquid conductivity curve (LCC). A generic material thus provides an approach to represent a group of individual materials within a cluster. This allows to select the generic cluster material for a case study, based on the type of brick (e.g., historical brick with clay, loam, sand) without extensive experimental characterization. Hence, the question rises to what extent the generic cluster material represents the constituent bricks of the cluster and the associated degradation risks. The original clustering analysis by Zhao was performed with 23 historical brick types but only 15 are fully available in the IBK material database and could be implemented in this study. The brick types are referred to as ZA to ZQ, Z standing for 'Ziegel' i.e., 'brick' in German and the second letter was used as an identification method. The physical properties for the brick types are summarized in Table 1 below.

Table 1: Physical properties bricks ZA -> ZQ, Zhao (2012)

N.	RHO	CE	Θ_{Por}	Θ_{Eff}	Θ_{Cap}	$\Theta_{80\%}$	LAMBDA	AW	MEW	KLEFF
	kg/m³	J/kgK	m³/m³	m³/m³	m³/m³	m³/m³	W/mK	kg/m²s$^{0.5}$	-	s
ZA	1835.620	814.592	0.307	0.283	0.170	0.005	0.528	0.182	15.662	2.91E-11
ZB	1769.170	1000.000	0.349	0.334	0.240	0.009	0.789	0.150	8.557	1.72E-09
ZC	1904.380	847.362	0.281	0.212	0.148	0.003	0.808	0.172	22.878	1.83E-09
ZD	1619.510	953.143	0.389	0.361	0.256	0.004	0.403	0.381	10.473	2.09E-09
ZE	1657.180	906.973	0.375	0.357	0.254	0.005	0.574	0.215	12.823	8.78E-10
ZF	1975.670	845.982	0.254	0.169	0.127	0.007	1.012	0.017	41.065	5.90E-11
ZG	1715.150	920.215	0.356	0.322	0.231	0.007	0.543	0.137	22.169	8.64E-10
ZH	1851.890	794.094	0.301	0.283	0.209	0.002	0.659	0.262	12.031	2.90E-09
ZI	1736.440	881.308	0.345	0.320	0.314	0.017	0.456	0.034	21.335	3.03E-09
ZK	1734.110	919.247	0.346	0.324	0.250	0.015	0.657	0.107	24.504	2.47E-09
ZL	1676.500	933.847	0.367	0.344	0.266	0.005	0.522	0.357	13.248	1.96E-08
ZM	1769.170	917.444	0.351	0.339	0.313	0.004	0.642	0.117	19.094	5.24E-09
ZO	1881.730	827.249	0.290	0.193	0.166	0.004	0.838	0.068	46.211	3.37E-08
ZQ	1948.050	813.169	0.265	0.179	0.162	0.003	0.905	0.022	98.636	1.11E-07

Response behavior, Heat Air Moisture modeling

In this study, the response behavior of masonry walls was evaluated using hygrothermal modeling. Heat Air Moisture (HAM)-simulations were performed according to EN 15026 with the Delphin 5.9 software from IBK (Institut Bauklimatic, Technical Universtity of Dresden) (Andreas and Grunewald, 2006; Grunewald, 2003). The hygrothermal behavior of a 1-dimensional setup is calculated by discretizing its geometry and defining the heat- and moisture transport for each cell. The transport depends on the material properties and the applied boundary conditions at the interior and exterior surfaces of the structure. In this study, the outside climate boundary condition was fixed at the test reference year (TRY 2011) of Essen located in Germany. A TRY includes hourly data for: atmospheric counter radiation, direct and diffuse radiation, wind velocity, wind direction, rain flux density on a horizontal surface, exterior temperature, and exterior relative humidity. In addition, the long wave emissivity was fixed at 0.9. At the exterior, the convective heat and vapor transfer coefficient were respectively set to 25 W/m²K and 2.10^{-7} s/m, whereas the indoor coefficients were respectively fixed at 8 W/m²K and 3.10^{-8} s/m. The interior climate boundary condition was calculated using the Delphin generator based on EN 13788 and is related to the governing outside temperature. To implement settling differences and initial conditions, two conditioning years were simulated. The 3-dimensional assembly including mortar, cracks, glue etc. can be represented quite accurate by an individual volume of continuous 1-D historic brickwork for real climate conditions (Vereecken and Roels, 2013). There may be discrepancies on this assumption where the impact of the interface resistance becomes significant (Zhou, 2020; Gutland, 2021) but is not the intention of this paper to make absolute statements about individual cases. The studied historical wall assemblies comprised a single leaf masonry with a plaster finish on the inner surface. The numeric outputs of the 3rd simulation year provided the

necessary temperature, relative humidity, and moisture data to perform degradation analysis. For the post processing and the of decay, Matlab software was used, and the results were visualized within the statistical R-software environment.

Case sampling

Different sets of sampled cases were constructed to address separate research questions. The first sample set adopted fixed brick properties according to the original values, summarized in Table 1. The remaining wall properties i.e., thickness and rain exposure were varied. The thickness of the brick wall was sampled between 150 and 500 mm. The orientation and rain exposure of a wall assembly are correlated and therefore, only the rain exposure was considered variable. The orientation was set to a West orientation, as it is the most critical regarding rain loads. The rain exposure varies in practice depending on the building geometry, height, location on the façade and wind orientation, and ranges in the simulations between 0 and 2 to respectively incorporate overhanging roofs and bad detailing of gutters. The first sample set is used to evaluate the original clustering analysis by Zhao. In the second sample set, brick properties were sampled while the wall thickness was fixed at 320 mm and the rain exposure set to 1.5. This sample set reduces the impact of wall related phenomena and focuses mainly on the impact of brick properties itself. In the third sample set both wall and brick properties were varied within the range defined in the first two sets. This sample set allows the most realistic comparative study between brick types. It is important that minor defects in experimental measuring processes as well as the natural variability within a single material are included during sampling. Therefore, a small variance was introduced by means of Latin hypercube sampling around the physical material properties of the original bricks. The width of the spread was based on the standard deviation for each individual property based on the 15 bricks, divided by a constant value of 5. The latter kept the spread small enough to prevent interweaving between the different original bricks but still represented a meaningful variance according to brick tests performed for an extensive case study (Calle, 2020). The variance was introduced on the material functions, i.e., the moisture retention (MRC) as well as the liquid conductivity curve (LCC), by normalizing the original function and applying a scaling factor, respectively the effective moisture content (θ_{eff}), and the liquid conductivity at effective moisture content ($K_{\theta eff}$). By doing so, the shape of the curves was respected but a small variance was introduced through the scaling factors. An example of the spread is shown in Figure 1.

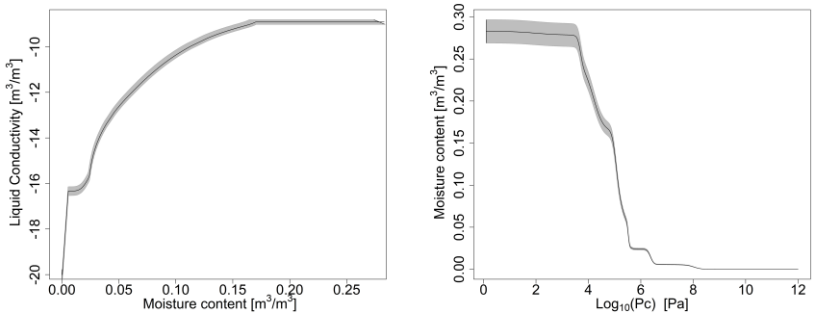

Figure 1: Spread on the material functions for brick ZA: MRC on the right and LCC on the left

All sample sets were developed with a minimum sample size of 500 cases per brick, which is an adequate sampling size according to Calle (2020). An overview of the different sampling sets and their assumptions is provided in Table 2 below.

Table 2: Summary of developed sample sets and assumptions

Variable		Sample Set 1	Sample Set 2	Sample Set 3
Wall thickness	[mm]	[150-500]	320	[150-500]
Rain exposure coeff.	[-]	[0-2]	1.5	[0-2]
Density	[kg/ m³]	Fixed	Variable	Variable
Heat Capacity	[J/kgK]	Fixed	Variable	Variable
Thermal Conductivity	[W/mK]	Fixed	Variable	Variable
Open Porosity	[m³/ m³]	Fixed	Variable	Variable
Effective moisture content	[m³/m³]	Fixed	Variable	Variable
Absorption coeff.	[kg/m²s$^{0.5}$]	Fixed	Variable	Variable
Vapor diffusion coeff.	[-]	Fixed	Variable	Variable
Liquid conductivity at effective moisture content	[s]	Fixed	Variable	Variable
Sample size	[-]	15x500	15x500	15x500

Determination of similar response behavior

In the second part of this study, similar response behavior was determined based on equivalences within the degradation profiles. This was done with several statistical sensitivity analyses. IEA Annex 55: Subtask 2 (Hagentoft, 2013) provides a clear list of several statistical methods to perform sensitivity analyses, each with their advantages and disadvantages. Zhao used standard regression, partial correlation coefficients and stepwise regression analysis in his research (Zhao, 2012). Calle questioned the suitability of these analyses since a strong non-linear behavior can be observed for brick properties (and in general for porous materials). Therefore, Calle added three analyses: the Spearman rank correlation, the scatterplot, and the Poison distribution-based classification trees (Calle, 2020). In this research paper, the Spearman rank correlation was calculated, and the results are represented with a horizontal bar plot. The further the bar reaches, the higher the impact of the specific material property. The plot is accompanied with p-values, if the value for a specific property surpasses the threshold of 0.05, it is confirmed as a non-significant variable. Scatterplots comprise no implicit assumptions and provide the reader with a quick grasp on the behavior of properties and their relation to the severity of degradation. In the evaluation of scatterplots, each individual dot represents a degradation level, and the color scheme is used to identify the 15 different bricks. Finally, segmentation-based sensitivity analysis techniques showed valuable to help define equivalences. Binary Poison distribution-based classification trees were adopted in this paper since the assumption for linearity and monotony are reduced to a minimum. Such a tree is generated by dividing the datasets into smaller subsets with increasing homogeneity. Consequently, the physical property with the largest impact on the heterogeneity of degradation is listed on top of the classification tree.

Three different performance criteria related to degradation were considered in this study: first, the formation of mould on the inner contact surface was predicted with the updated VTT model by Hukka and Viitanen (1999). Mould endangers the occupants' health by introducing respiratory complaints, headaches, allergenic nausea and should be controlled in a correct fashion (ASHRAE, 2009; Hukka and Viitanen, 2011; Vereecken and Roels, 2012; Viitanen et al, 2007, 2011). Secondly, historic masonry facades often provide a load bearing support for wooden beams which are vital as structural support in the flooring system (Brischke, 2008, 2011, 2016, 2019; Kehl, 2013; Vanpachtenbeke, 2019; Vereecken and Roels, 2019). So, wood deterioration of these beam heads could render the structure vulnerable for failure and collapse. In this research paper, the occurrence of brown wood rot was calculated using the prediction model by Brischke and Rapp (2008, 2019). The model is based on field testing of samples throughout Europe. Finally, frost damage could damage the outer parts of the brickwork and therefore the formation of ice was predicted at 5 mm of the exterior wall surface (Fagerlund, 1975; Mensinga et al, 2010). To quantify the increase or decrease in frost damage, the criterion for freeze-thaw-cycles according to Mensinga et al (2010) was adopted.

Mould growth

There are different mould prediction models, the authors refer to Vereecken and Roels (2012) for an overview and evaluation of these models. In this study, the mould growth on the inner surface of the wall structure was predicted by the updated VTT model by Viitanen (1999, 2007) as it considers mould initiation, growth rate as well as decline during dryer periods. It comprises a dynamic model related to two time-depending variables: relative humidity and the temperature on the surface. The severity of the mould is presented by a mould index ranging from 0 to 6 with increasing degradation according to Table 3.

Table 3: Mould Index Classification table (Viitanen et al, 2007)

Index	Growth rate	Description		
0	No mould growth	Spores not activated		
1	Small amounts of mould on surface	Initial stages of growth	Microscopic level	
2	< 10% coverage of mould on surface			
3	10-30% coverage of mould on surface Or < 50% coverage of mould (microscopic)	New spores produced		Visually detectable
4	30-70% coverage of mould on surface Or > 50% coverage of mould (microscopic)	Moderate growth		
5	> 70% coverage of mould on surface	Plenty of growth		
6	Very heavy, dense mould growth covers nearly 100% of the surface	Coverage around 100%		

First, the critical relative humidity is defined, representing the minimum humidity at which initiation of mould growth starts when exposed for a prolonged period of time.

$$RH_{crit} = \begin{cases} -0.00267\,T^3 + 0.16\,T^2 - 3.13\,T + 100 \; when \; T < 20℃ \\ RH_{crit} \; when \; T > 20℃ \end{cases} \quad (1.)$$

The increase or decline in the mould formation is calculated by the use of a differential equation with time steps expressed in hours. In the equation the varying temperature and relative humidity can be included for a more complete assessment.

$$\frac{dM}{dt} = \frac{k_1 k_2}{168\ (\ -0.68\ln(T) - 13.9\ln(RH) + 0.14W - 0.33SQ + 66.02)} \quad (2.)$$

The factor k_1 defines the intensity of the growth whereas W is depending on the timber species (0 for pine and 1 for spruce), SQ implements the surface quality in the assessment (0 for a sawn surface and 1 for kiln dried quality). k_2 defines the moderation of the growth when the mould index approaches the maximum peak level of mould.

$$k_2 = \max\left[1 - \exp[2.3(M - M_{max})], 0\right] \quad (3.)$$

In the latter, the maximum mould index depends on the governing relative humidity and temperature:

$$M_{max} = A + B.\frac{RH_{crit} - RH}{RH_{crit} - 100} - C.\left(\frac{RH_{crit} - RH}{RH_{crit} - 100}\right)^2 \quad (4.)$$

The original model of Viitanen was based on pine sapwood, in an improved model (Viitanen and Ojanen, 2007) the assessment for other materials was added. Hence the following factors in the equations: k_1, k_2, A, B and C. These are depending on the sensitivity level of the material. Different sensitivity classes are defined in Table 4 and the corresponding parameters can be found in Table 5.

Table 4: Mould sensitivity classes (Ojanen et al, 2010,2011)

Sensitivity class	Materials in experiment	Material groups
Very sensitive (vs)	Pine sapwood	Untreated wood; includes lots of nutrients for biological growth
Sensitive (s)	Glued wooden boards, PUR with paper surface, Spruce	Planed wood; paper-coated products, wood-based boards
Medium resistant (mr)	Concrete, aerated and cellular concrete, Glass wool, polyester wool	Cement or plastic based materials, mineral fibers
Resistant (r)	PUR with polished surface	Glass and metal products, materials with efficient protective compound treatments

Table 5: Parameters for different mould sensitivity classes (Ojanen et al, 2010,2011)

Sensitivity Class	k_1 (if M<1)	k_2 (if M ≥ 1)	M_{max} (influence on k_2) A	B	C	RH_{min} (%)
Very sensitive (vs)	1	2	1	7	2	80
Sensitive (s)	0.578	0.386	0.3	6	1	80
Medium resistant (mr)	0.072	0.097	0	5	1.5	85
Resistant (r)	0.033	0.014	0	3	1	85

When the mould fungi are not exposed to sufficient moisture or temperature levels, the growth rate does not remain constant but will decrease during these dry periods. A finite delay in mould growth is clearly noticeable after the dry period. The delay is described by the mathematical description dependent on time, starting from the beginning of the dry period $(t - t_1)$.

$$\frac{dM}{dt} = \begin{cases} -0.000133, & when\ t - t_1 < 6h \\ 0, & 6h < when\ t - t_1 < 24h \\ -0.000667 & when\ t - t_1 > 24h \end{cases} \quad (5.)$$

Eq. (5.) can take slightly different values for periods longer than 14 days and temperatures below 0 °C due to the small number of testing samples in the original test. Also, the material and its sensitivity level for mould will have a significant influence on the mould decline rate. This influence is implemented using a constant value relative to the material. In the case of historic brick material almost no decline (C_{eff} = 0.1) was assumed during the analysis.

$$\frac{dM}{dt}_{mat} = C_{mat}\frac{dM}{dt}_0$$

Table 6: Decline rate parameters dependent on material (Ojanen et al, 2010,2011)

C_{eff}	Description
1	Pine in original model, short periods
0.5	Significant relevant decline
0.25	Relatively low decline
0.1	Almost no decline

The masonry of historic brickwork in this study was finished with a layer of historic plaster at the inner surface and according to Table 4, the class sensitive (s) was assumed during calculation. Note that when the wall is painted, it is possible that

sensitivity for mould growth is reduced when compared to glued wooden boards or a paper surface, due to mould resistance additives in the paint.

Wood degradation

Different types of organisms or fungi can attack wood. Wood decaying fungi consume cell wall material and thus negatively affect the structural properties of timber elements (Vanpachtenbeke, 2019). Vanpachtenbeke listed different wood decaying prediction models and concluded that reliable prediction models for wood degradation are scarce and divided in static laboratory and dynamic field testing. In this paper the experimental testing on Scots Pinewood by Brischke and Rapp (2008, 2019) was used, as it is the only model that incorporates the onset of wood decay. In the calculations it was assumed that the wooden beams embedded in the wall are exposed to the same relative humidity and temperatures gradients as the surrounding brickwork. Consequently, deterioration was calculated using the conditions of the surrounding brickwork. Without modeling the wooden element, the computational time was reduced as a 1-dimensional geometry could be applied. In the adopted prediction model of Brischke and Rapp, the impact of governing moisture content and temperature on the onset and growth of wood decay is described by a dose-response function. Daily dose, D, is calculated with a temperature induced component D_T, in which the temperature [°C] is averaged over a timespan of a day, and a moisture content induced component D_{MC} dependent on the daily average moisture content [%]. The necessary parameters were defined at a location of 120 mm from the inner plaster surface using HAM simulations. The distance represents the typical load bearing support for the beam structures.

$$D = \frac{a.D_T(T) + D_{MC}(MC)}{a+1} \qquad if\ D_{MC} > 0\ and\ > 0 \tag{6.}$$

$$D_T(T) = \begin{cases} 0 \\ k.T^4 + l.T^3 - m.T^2 + q * T \end{cases} \qquad \begin{matrix} if\ T < 0°C\ or\ T > 40°C \\ if\ T > 0°C\ and\ T < 40°C \end{matrix} \tag{7.}$$

$$D_{MC}(MC) = \begin{cases} 0 \\ e.MC^5 - f.MC^4 + g.MC^3 - h.MC^2 + i.MC - j \end{cases} \qquad \begin{matrix} if\ MC < 25\% \\ if\ MC \geq 25\% \end{matrix} \tag{8.}$$

The results of the prediction model and the experimental results from field testing were fitted with a Gompertz function and described with a wood degradation rating for the assessed Scots pine sapwood. In this paper, the prediction model for brown rot was used, as brown rot generally proceeds faster and hence provides a conservative approach and allows better differentiation between cases (Brischke and Rapp, 2008).

$$DR\big(D(n)\big) = 4.\exp\left(-\exp\Big(1.7716 - \big(0.0032 * D(n)\big)\Big)\right) \tag{9.}$$

Table 7: Decay rating according to EN 252 (CEN 2014)

Rating DR	Classification
0	No attack
1	Slight attack
2	Moderate attack
3	Severe attack
4	Failure

Research by Vereecken and Roels (2019) showed a significant increase in the risk of wood decay when the airtightness around the beam head is not secured. The exfiltration of humid indoor air can create a favorable environment for decaying organisms. In this paper an airtight seal around the beam head was assumed.

Frost decay

The degradation induced by freezing water is highly debated among researchers. Three possibilities to calculate decay are: the number of critical freeze-thaw-cycles (FTC), the ice mass density, and the hygric and thermal stress in the material. The built-in calculation of freeze-thaw-cycles in Delphin 5.9 is either based on governing temperature or ice mass volume (Andreas and Grunewald, 2006, Grunewald, 2003). In the temperature-based calculation, a freeze-thaw-cycle starts when the temperature drops below dewpoint. In the ice mass volume method, a cycle is counted when the ice mass density over pore volume surpasses a threshold boundary level. The last method was used in this study with the limit set to 25%, based on the study of Mensinga et al (2010). Mesinga indicated that the critical degree highly depends on the pore structure, which implies that the criterion is different for each brick type and evidently complicates this comparative study. The Delphin 5.9 software model is based on a thermodynamic equilibrium between the water content in the ice phase and the liquid phase, leading to an equation where, as a function of the temperature below dewpoint, the capillary pressure occurring in the largest non-frozen-pores is described. With the aid of this relation, it is possible to determine the frozen and unfrozen water content. An important change in capillary suction is introduced due to the decrease of liquid water content in the pores during the

formation of ice. Hence, the transport of liquid water towards the ice volume is considered until the complete free pore structure is filled. Note that the calculation of the ice volume is based on the occurring capillary pressure in the pores, and thus the dewpoint depression is considered (Andreas and Grunewald, 2006; Grunewald, 2003). In this paper, the frost damage was assessed at a depth of 5 mm from the exterior surface.

Results

Part 1: Response behavior of Zhao's clustering analysis

In the first section, the clustering analysis according to Zhao was performed on the 15 available bricks. The result was almost identical to the results reported by Zhao and the small differences can be explained by the lack of information of the remaining 8 brickworks as they are excluded from the Delphin database. Subsequently the response behavior regarding degradation within an individual cluster was compared based on HAM simulations of sample set 1. A summary of the response behavior for all 19 bricks (15 original, 4 generic) is visualized in Figure 2. The different clusters are marked by a surrounding red box on the X-axis and the generic material is marked by the capital c accompanied with the cluster identification number. In Figure 2, the distribution for each degradation criterion is given for all individual brick types, what allows to compare the response behavior within one cluster. In the comparison for mould growth, the response behavior within a cluster lacks homogeneity, especially for clusters 2 and 4. The most critical difference was noticed in cluster 4 where brickwork ZC and ZF were clustered together while the mould index shows a difference of three units. The latter represents a difference in mould coverage from 0% to a coverage of 50%. A similar observation was made for wood deterioration. Here, the most critical case was noticed in cluster 2 where brickwork ZK showed significant higher wood decay compared to the remaining cluster elements i.e., brickwork ZB, where almost no wood decay was observed. The largest difference for frost damage was observed in the same cluster. Brickwork ZB showed significantly lower freeze-thaw-cycles than the average of the cluster. The prediction of the response behavior within a cluster by means of a generic material is reported in the same figure. For all performance criteria the response behavior for a generic material cannot be used as a representation of those of the constituent materials. For renovation assessment, these differences in degradation profiles could lead to an incorrect prediction of performance and should be considered with great care. Clustering analysis performed with equally weighted material properties is consequently no guarantee for correct representation and associated risk assessment.

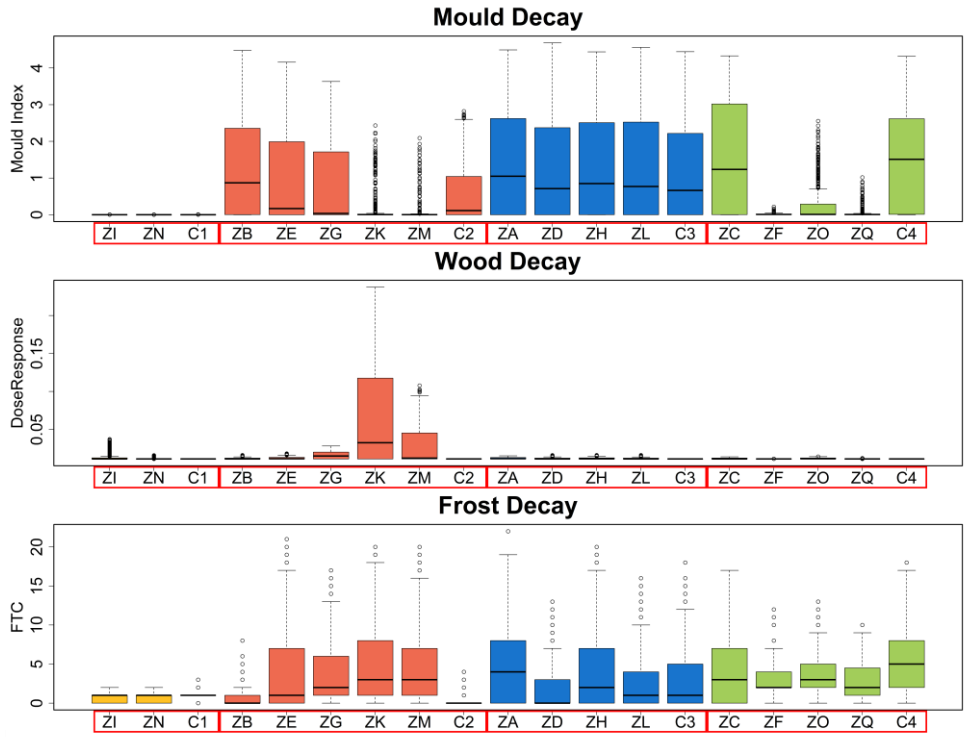

Figure 2: Analysis of homogeneity clusters derived from Zhao's approach (2012) for the different degradation models for 15 brick types and 4 generic cluster materials (Mould decay, top; Wood decay, middle; Frost decay, bottom)

Part 2: Definition of similarities in response behavior

In the second part of this study a methodology was developed for each degradation model to determine the relation between similar response in behavior and similarity in material properties. The overarching aim of this study was to push the potential and application of clustering approaches in practice by including the response behavior. To reflect these projects in the most comprehensive way, sample set 3 was used. Here, material properties as well as wall related properties were varied to represent the inherent variability and uncertainties in practice. To start the comparative study the distribution of moisture throughout the different brick types was evaluated in Figure 3, where field plots show the moisture content for a one-year period. For each brickwork the plot on top represents a wall assembly of 500 mm, whereas the plot below shows the result for a 200 mm thick wall. In addition, the field plots are ranked with rising absorption coefficient, from the top left to the right bottom corner. One can see that brickwork remains wet throughout the winter period, and for higher absorptive brick types, dries out fast during summer periods. The outer centimeters of the brickwork dry out differently due to convective drying, which can cause a different response behavior for frost damage. The impact of absorption on the moisture behavior is demonstrated for brickwork ZF and ZD, representing the largest difference in absorption coefficient. For a lower absorption, the infiltration depth of the liquid moisture front is reduced, but also the drying rate is slowed down, resulting in a higher moisture mass density over summer. In conclusion, the water infiltrated much deeper for high absorptive bricks and coupled with a fast-drying rate, resulted in an almost constant moisture redistribution over the complete depth in a single time frame. The latter is in contrast with low absorptive bricks where larger gradients were noticed across the wall. Subsequently, homogeneity in response behavior for the individual performance criteria was evaluated with sensitivity analyses.

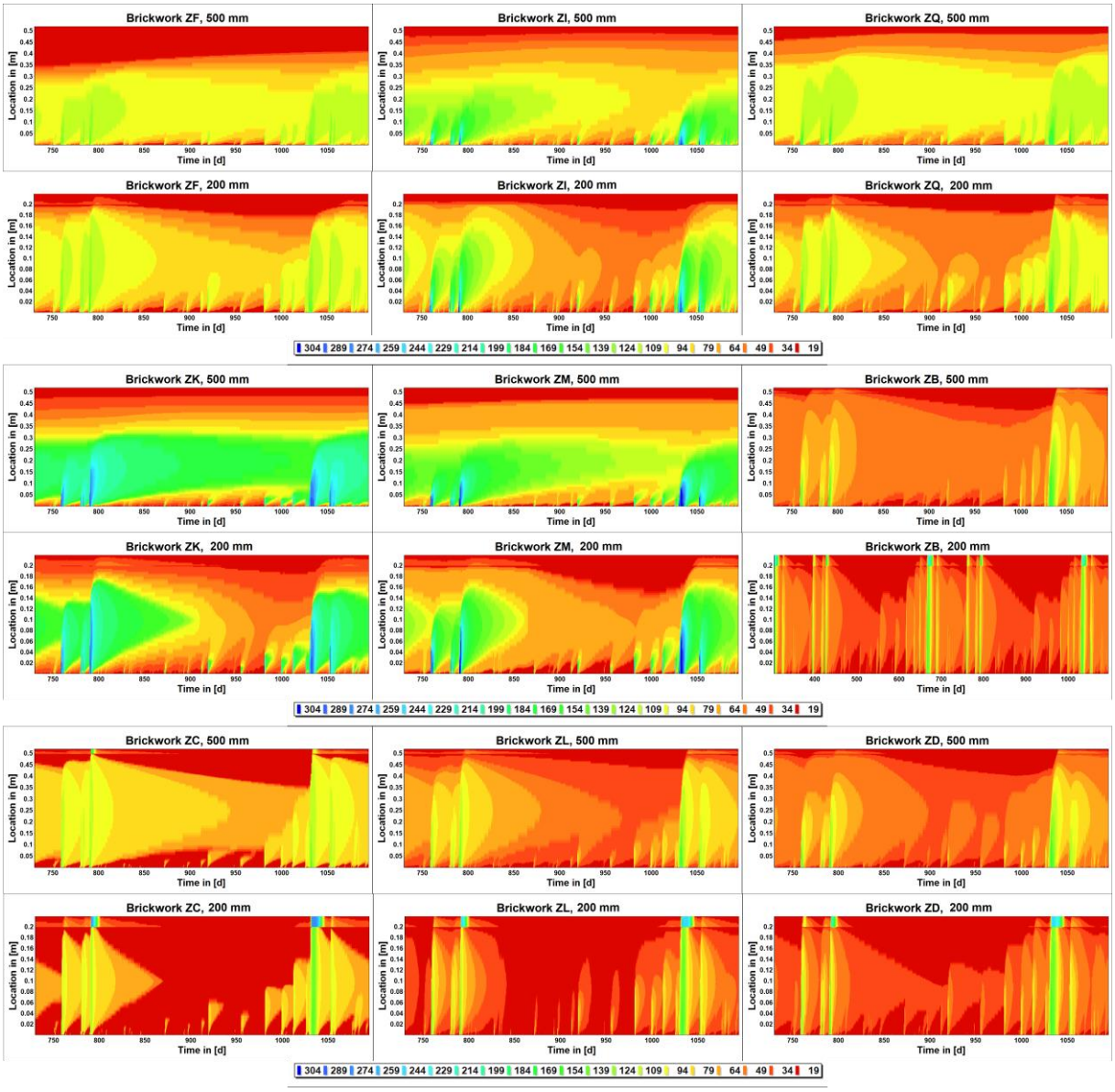

Figure 3: Field plots for walls with 9 different bricks, showing the evolution and distribution of the moisture content for a 1-year period.

Mould Index

The mould index according to the improved VTT model developed by Viitanen (1999, 2007, 2011) was calculated on the inner surface of the interior plaster. The type of applied plaster was evaluated in a separate analysis based on four different plasters and showed a negligible impact on the mould growth. With the help of sensitivity analyses based on the material and wall properties, reported in Figure 4-6, similar response behavior for the different bricks was determined. It can be observed that the rain exposure coefficient is consistently the dominant parameter for mould growth risk. Hence, this parameter is ranked on top in the classification tree in Figure 4. As the exposure defines the amount of rainwater, which is projected onto the wall, it also defines the maximum value that can be absorbed. The spearman rank in Figure 5 shows the impact for the considered values for three brick types which are ranked from left to right according to rising absorption coefficient. The impact of the thickness reduces when the brick exhibits a higher absorption. This trend can be explained with the field plots ZF and ZD in Figure 3. For ZD, the infiltration depth of the waterfront was not affected by thickness whereas for ZF a clear impact from the thickness can be seen. There, for a thicker wall the infiltration depth was lower, and the waterfront did not reach the interior plaster. Conversely, the moisture was redistributed towards the middle of the brickwork, creating dryer conditions for the interior plaster and lower mould growth. The scatterplots in Figure 6 show the mould index for each sample for the 15 brickworks. Again, the dominant impact of the rain exposure was confirmed. Focusing on the physical properties of the bricks in the classification tree and scatterplots, a clear subset division was noticed for a threshold absorption coefficient of 0.128 $kg/m^2s^{0.5}$. It was found that lower absorbing brick types showed a higher resistance to mould whereas the higher absorbing brick types were exhibiting a higher mould index.

Furthermore, Figure 8 and Figure 9 evaluate the impact of the inherent drying rates and material functions i.e., the moisture retention curve (MRC) and the liquid conductivity curve (LCC). The top plots show the magnitude of degradation as a function of capillary pressure and moisture content and the bottom plots show the occurrence of mould growth plotted on the moisture retention and liquid conductivity curve. Two examples were selected: brick type ZM which showed limited mould growth and ZC which showed larger traces of mould. The results were obtained by simulating a wall assembly with fixed brick properties, a thickness of 200 mm and a rain exposure of 2. On each material function, the critical moisture content, θ_{crit}, obtained with a simulated drying test is indicated by means of a blue dot. The θ_{crit} represents the changing point between the first and second phase of the drying process. The first drying stage is represented by a linear mass loss over time, caused by convective drying through the porous material. In contrast, the second drying stage is dominated by diffusion of water vapor and consequently exponentially lowers the drying rate. For mould analysis not only the magnitude of the fungal growth is important, but also the duration will determine the severity of growth. The duration is mainly dictated by the length and intensity of a rain event and by consequence, by its geographical location. Note that the trend and shape of the moisture retention curve determines at which moisture content level the critical value of 80% RH for mould growth is reached.

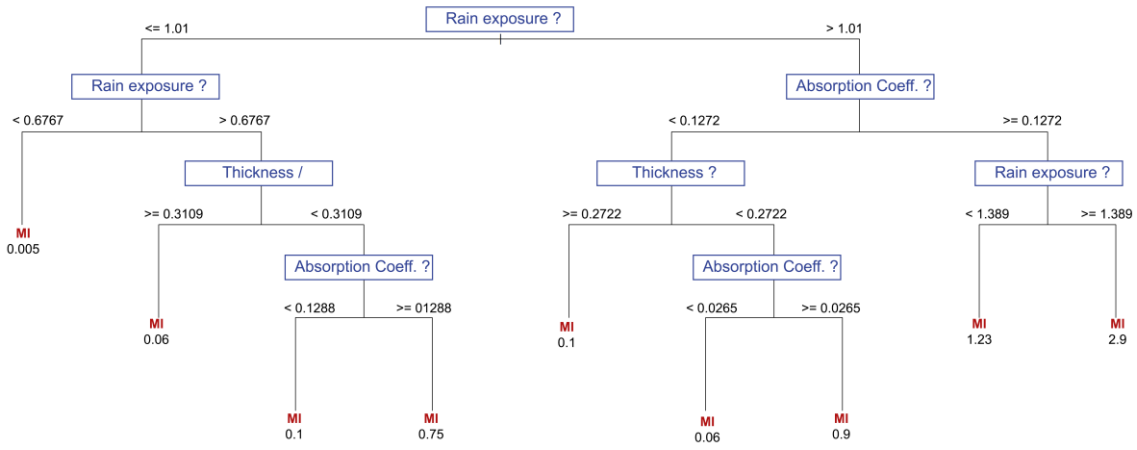

Figure 4: Classification tree for mould degradation`

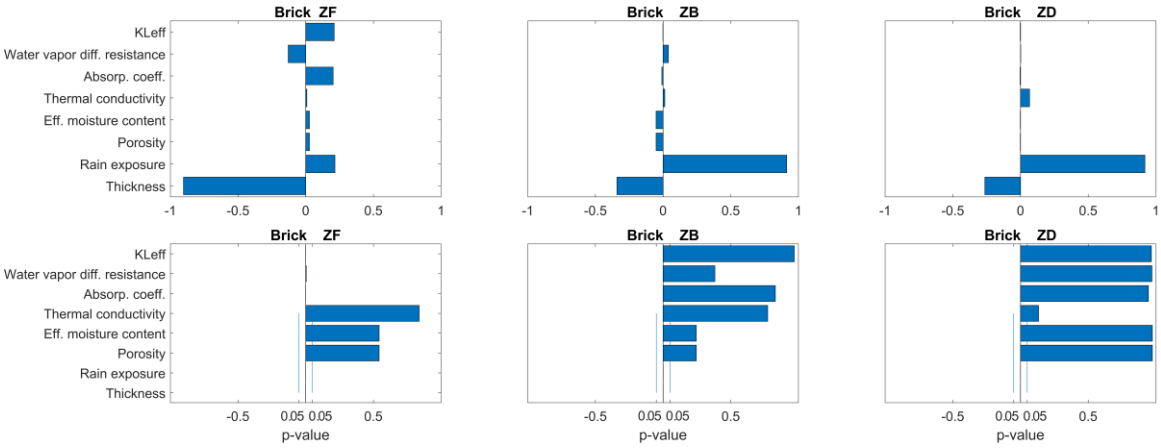

Figure 5: Spearman rank correlation for mould degradation in three different brick types, ranked with increasing absorption coefficient

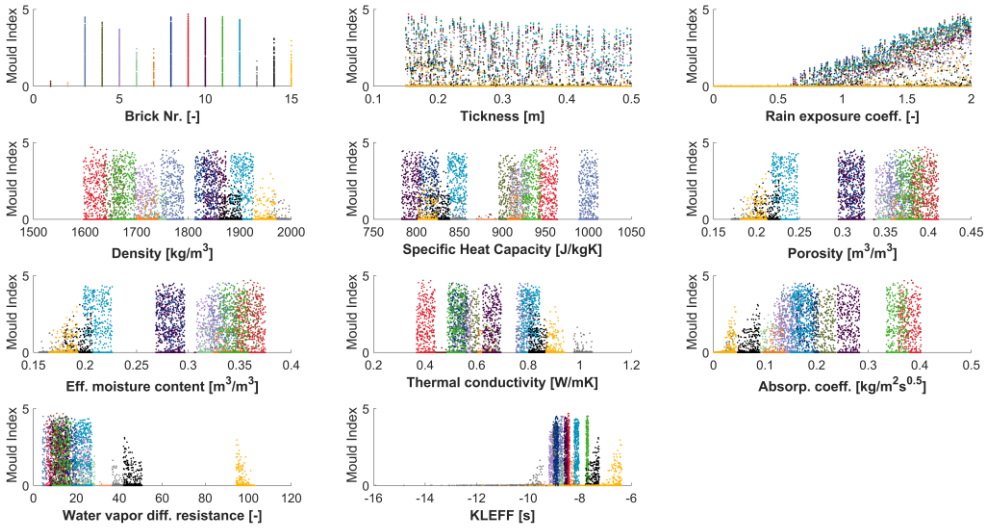

Figure 6: Scatterplot for mould degradation based on Mould Index, color code per brick type

In conclusion, to obtain a similar mould response among bricks, the wall properties were neglected and the brick dependent absorption coefficient A_w was found to be critical. Hence, the latter was considered the most valuable clustering parameter for mould resistance. When the degradation profiles were divided with threshold A_w = 0.128 kg/m^{2}s$^{0.5}$, the cluster scheme shown in Figure 7 was obtained. The red boxes represent the two clusters. Cluster 1, on the left, contains the low absorptive bricks where in general a low mould growth was observed. The second cluster which represents the high absorptive brickworks however, entails significantly larger traces of mould. In contrast to the clustering of Zhao (2012), where the absorption coefficient was considered as an equally weighted variable, this analysis highlights the key impact on the hygrothermal behavior and renders it the dominant parameter for clustering. This approach resulted in a more reliable methodology for clustering based on the combination of physical properties and response behavior of the material.

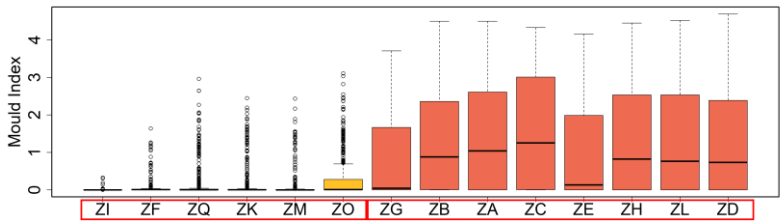

Figure 7: Clustering scheme of degradation profiles for mould degradation

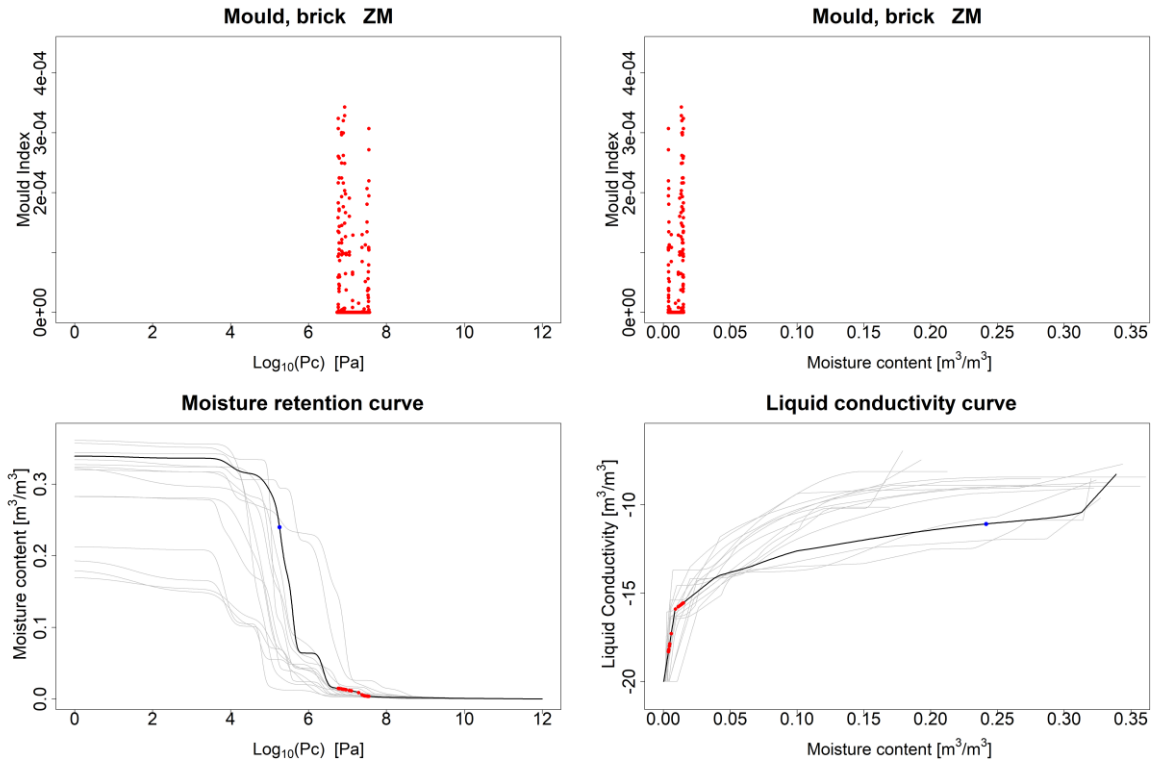

Figure 8: Top: Occurrence of mould growth as a function of capillary pressure and moisture content for a 200 mm wall of brick type ZM. Bottom: occurrence of mould growth plotted on the moisture retention and liquid conductivity curve for ZM

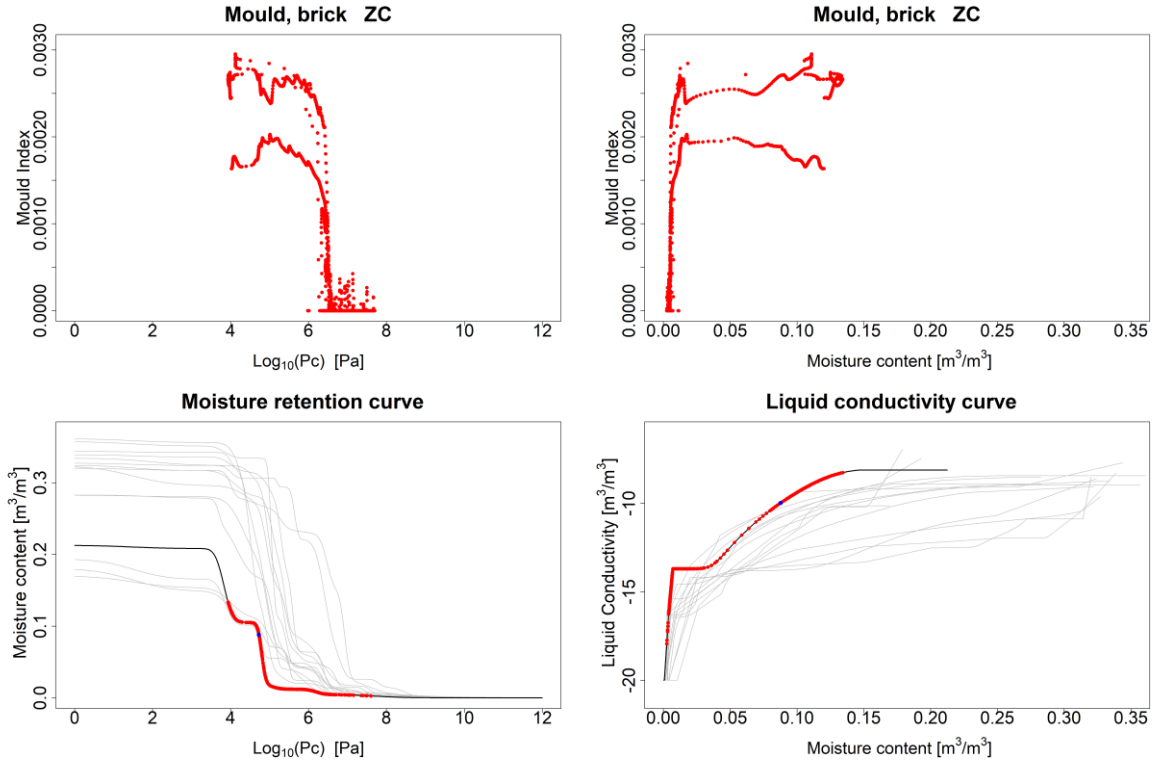

Figure 9: Top: Occurrence of mould growth as a function of capillary pressure and moisture content for a 200 mm wall of brick type ZC. Bottom: occurrence of mould growth plotted on the moisture retention and liquid conductivity curve for ZC

Wood degradation

The occurrence of wood rot was predicted with the numerical prediction model by Brischke and Rapp (2008, 2019) for an embedded wooden beam in a solid masonry wall. The calculation of the degradation requires the daily moisture content and temperature in the beam head, located at a fixed 120 mm from the interior surface. The assumption was made that a timber beam end is in equilibrium with its surrounding brickwork, allowing the assessment of wood degradation without modelling the beam element itself. The sensitivity analyses in Figure 10-12 showed similar results as for mould formation: the rain exposure coefficient yields the highest impact on the severity of woot rot. Based on the classification tree in Figure 10, the impact of the rain exposure can be generalized for all brick types. With increasing exposure, more rain can be absorbed by the wall, inducing a higher moisture content in the timber elements which in turn will lead to a higher daily dose of woot rot. The latter explains the increasing trend of the wood rot on the exposure scatterplot in Figure 12. A contradiction with the results for mould growth is found because wood decay shows a positive correlation with wall thickness. The field plot ZK in Figure 3 clarifies this correlation. For an increasing thickness, the moisture redistribution towards the inner wall was limited. This created a concentrated storage of moisture more towards the exterior and consequently raised the moisture and wood rot in the beam head. Figure 11 shows the decreasing impact of other brick related properties for higher absorptive brickwork. For example, in ZD, which is highly absorptive, other brick properties show to be non-significant. Therefore, it can be derived that for these types of bricks small variations or uncertainties will not affect the severity of wood deterioration. The classification tree as well as the scatterplots show a clear threshold around A_w 0.14 kg/m^{2}s$^{0.5}$. In the scatterplots, where each result of the sample is visualized by an individual dot, there is a negligible spread on the results for higher absorptive brick types. This confirms that for the latter the exact value is of lesser importance, and perhaps a simple on-site test can already indicate whether additional, more time-consuming, testing is required. For brickwork with lower absorptive properties, one should determine the brick properties with greater care as a larger spread in the results was observed. With the same methodology as for the mould formation, the impact of material functions and drying rate was evaluated using Figure 14-15, focusing on the moisture retention (MRC) and liquid conductivity (LCC). Here, ZK is a brick type with large susceptibility for wood rot, whereas brick ZL shows little wood decay. The capillary pressure at which wood degradation was initiated is similar for the two bricks. Moreover, the trend of the MRC in the direct environment of the initiation moisture content is almost identical. However, the LCC was considerably lower in the case of brickwork ZK and evidently relates to the absorption. Additionally, one can see that a large impact on wood rot is derived from the location of the critical moisture content θ_{crit} in relation to the moisture content at which wood decay is initiated (θ_{int}). When the θ_{crit} value is located higher in comparison to the θ_{int}, the degradation of wood rot occurs also in the slower second drying stage. This implies that the number of events where the cell wall material was attacked by brown rot, occurred at much higher frequency and in turn induced a higher density of daily doses.

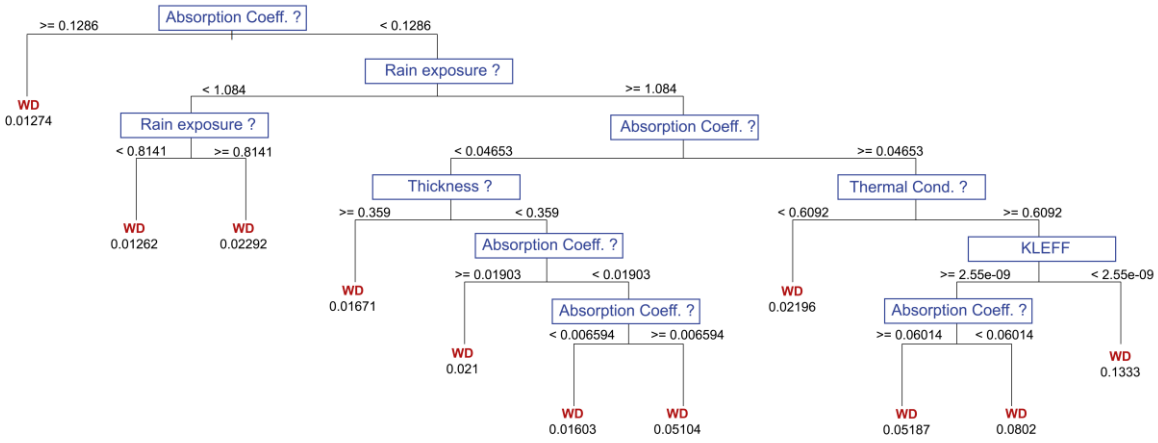

Figure 10: Classification tree for wood degradation

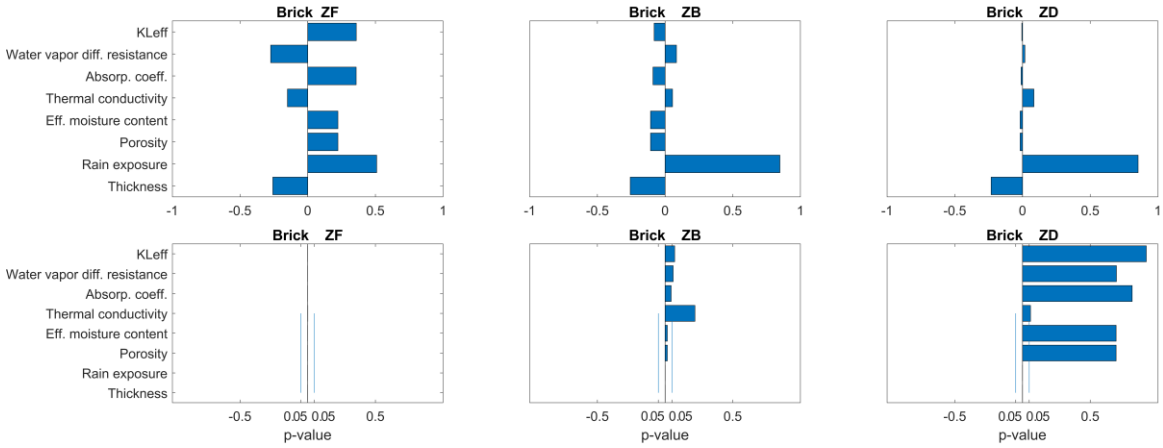

Figure 11: Spearman rank correlation for wood degradation, three different brick types, ranked with increasing absorption coefficient

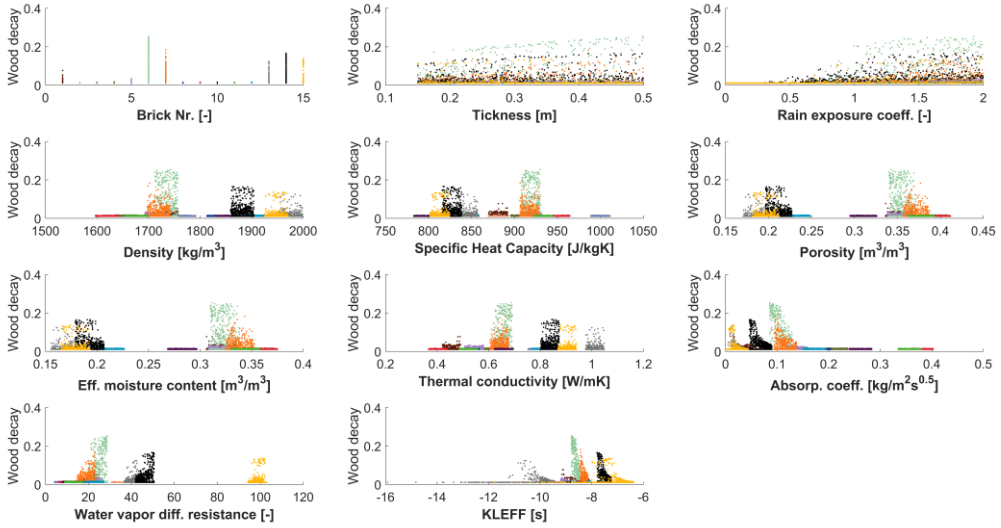

Figure 12: Scatterplot for wood degradation based on daily dose, color code per brick type

Similar to the study on mould risks, the wall related properties were neglected in the process of defining homogeneous response behavior. Based on the analyses above, the clustering scheme in Figure 13 was obtained. For wood rot, the absorption coefficient, liquid conductivity curve and critical moisture content showed a high reliability as clustering parameters. Consequently, a value of 0.14 kg/m^{2}s$^{0.5}$ for the absorption coefficient created two clusters, which are represented by two red surrounding boxes in Figure 13. Similar results were achieved when the location of θ_{crit} in relation to the θ_{int} was considered to define the clusters. It can be concluded that the newly obtained clustering incorporates similar wood response behavior while still representing a meaningful homogeneity in material properties.

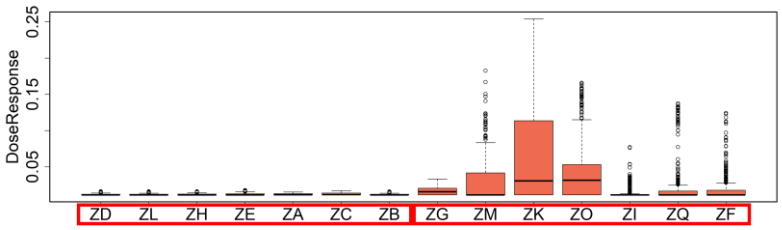

Figure 13: Clustering scheme of degradation profiles for wood degradation

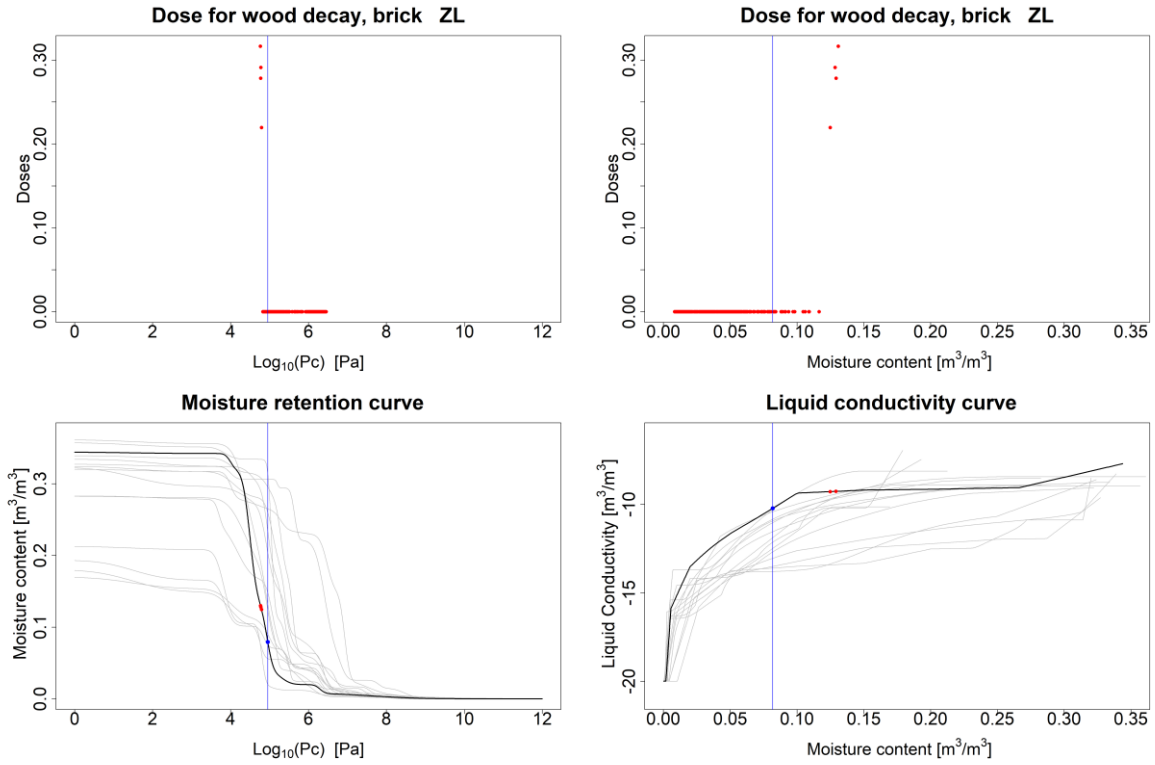

Figure 14: Top: Occurrence of daily dose for wood rot as a function of capillary pressure and moisture content for a 200 mm wall of brick type ZL. Bottom: occurrence of daily dose for wood rot plotted on the moisture retention and liquid conductivity curve for ZL

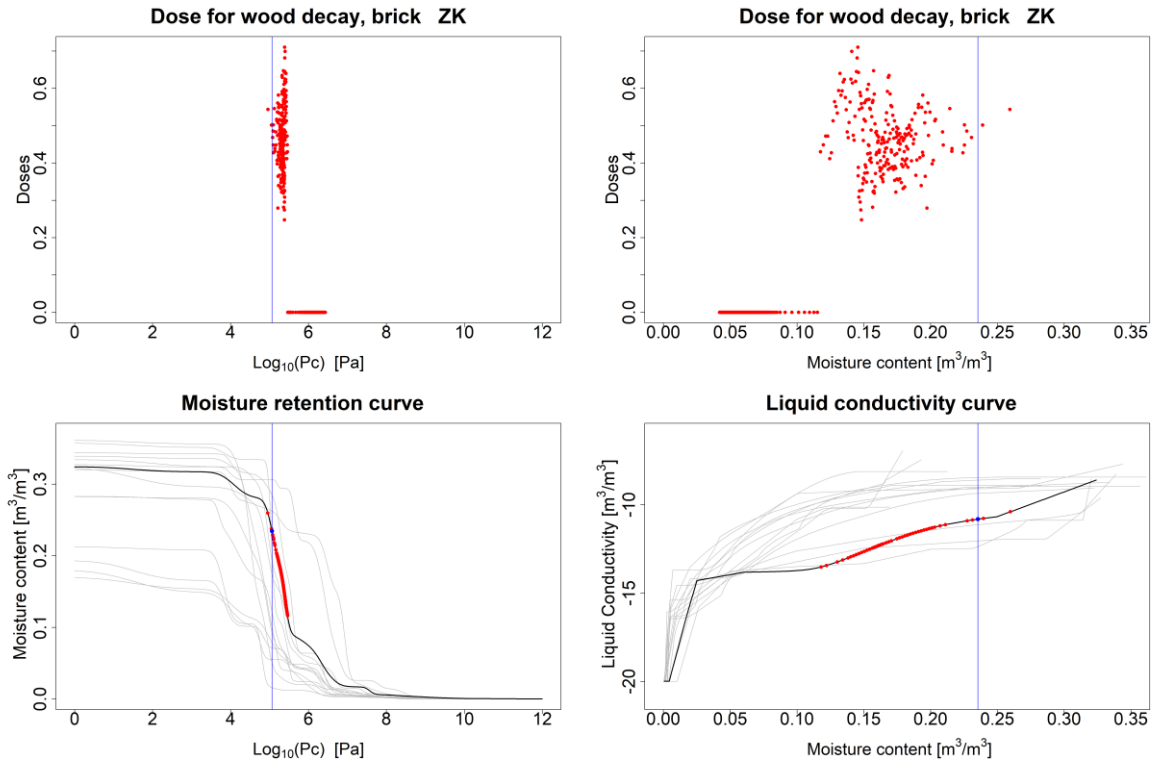

Figure 15: Top: Occurrence of daily dose for wood rot as a function of capillary pressure and moisture content for a 200 mm wall of brick type ZK. Bottom: occurrence of daily dose for wood rot plotted on the moisture retention and liquid conductivity curve for ZK

Frost degradation

Frost decay was determined with the count of freeze-thaw-cycles (FTC) with a threshold level of 25% ice volume according to Mensinga et al (2010). During analysis it became clear that fluctuations around the threshold increased the count drastically, but it is anticipated that these do not entail any significant change in inflicted damage. Therefore, the total cumulative ice volume above 25% was calculated as reference. The sensitivity analyses visualized in Figure 16-18, show a dominant behavior for the rain exposure on the FTC results. Reduced rainfall rates projected on to the wall might result in an insufficient liquid water content located in the pores to reach the threshold ice volume. Similar as for wood decay, an increased wall thickness limits the moisture ingress and causes moisture storage towards the exterior surface and consequently increased the ice volume in the exterior pores. The brick related properties absorption coefficient, water vapor diffusion resistance and density are dependent on the pore system, and according to the classification tree in Figure 16 these properties have a dominant impact on the severity of frost damage. A low absorption coefficient in Figure 17 and in Figure 18, shows a lower spread in the results and by consequence, small variations and discrepancies in measurements have a lower impact here. This can be explained by the way absorption is integrated in the HAM-modeling. The liquid conductivity curve was scaled with the $K_{\theta eff}$ which was calculated over a quadratic function of A_w. The latter results in a higher deviation and uncertainty when calculated with an absorption coefficient closer to zero. Figure 20-21 were constructed in a same way as for the previous criteria. Here, brickwork ZQ represents a higher frost decay whereas brickwork ZI represents a lower count of freeze-thaw-cycles. For the sensitivity analyses, in particular the classification tree in Figure 16 and the Spearman rank in Figure 17, the absorption coefficient was dominant. However, while brickwork ZQ and ZI have relatively similar absorption coefficients, considerable differences in their frost degradation profiles were noticed. In Figure 20-21, an alternative brick property was observed to be highly influential. When focusing on the moisture retention curve, one could observe a large difference in capillary pressure the moment a freeze-thaw-cycle was registered. The frost cycle in brickwork ZI was induced at much higher pC and since the depression of dewpoint was considered during the simulation, a lower temperature was required to initiate the ice formation process. Thereby, smaller pores were inducing the ice formation in the brickwork when the dewpoint was lowered.

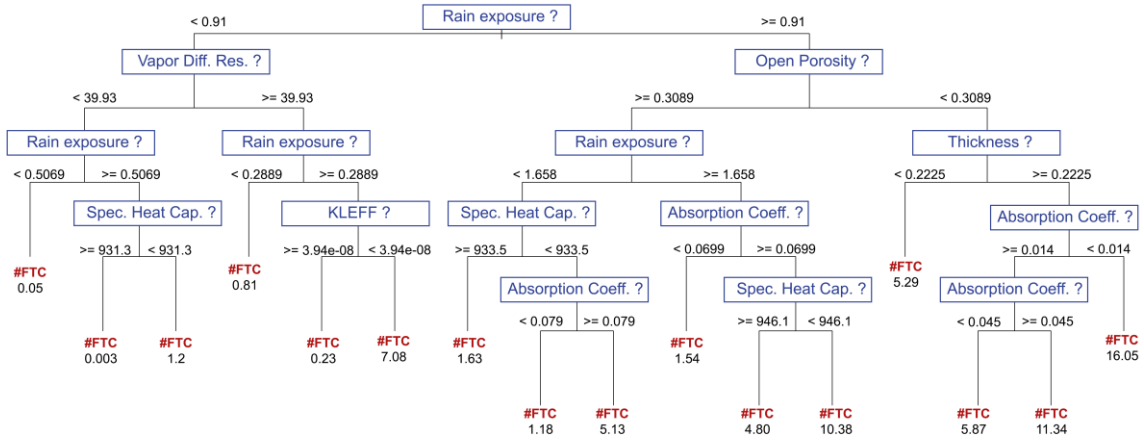

Figure 16: Classification tree for frost degradation

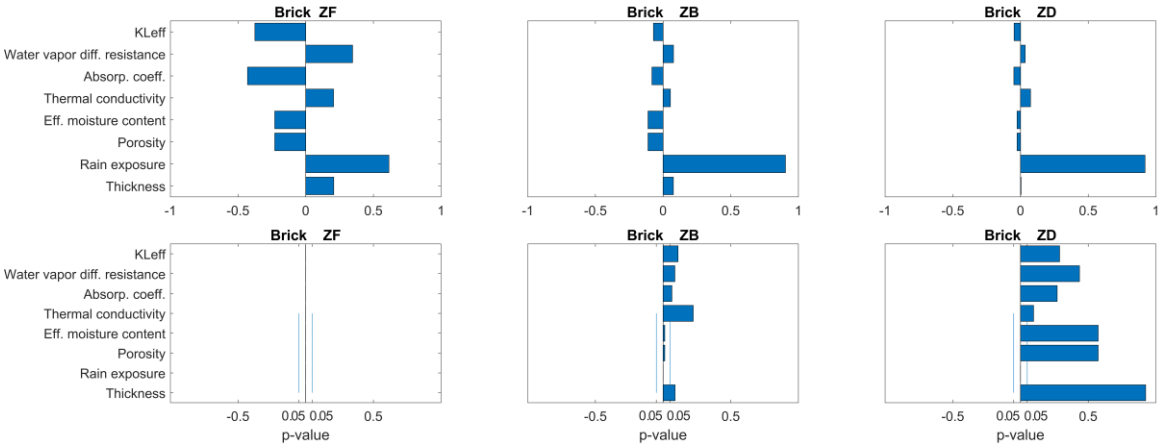

Figure 17: Spearman rank correlation for frost degradation, three different brick types, ranked with increasing absorption coefficient

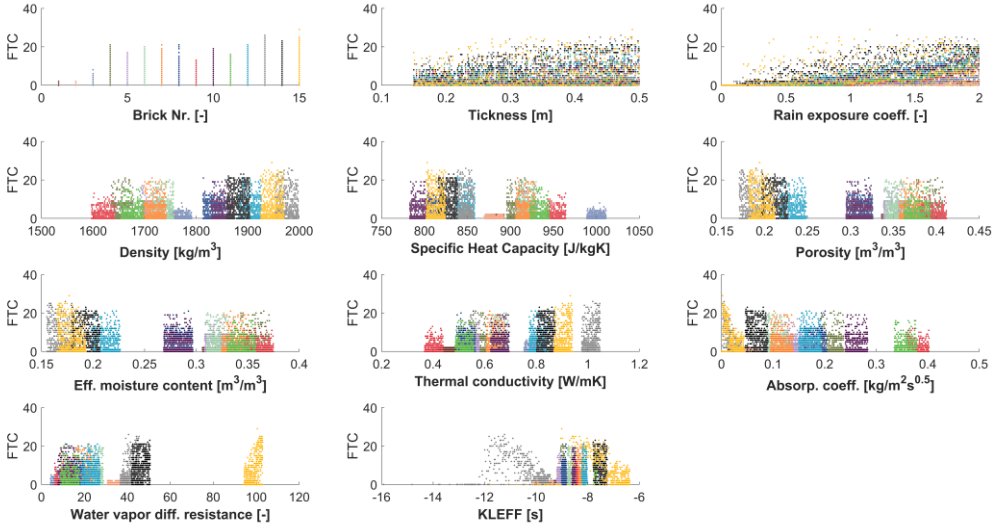

Figure 18: Scatterplot for frost degradation based on FTC, color code per brick type

After omitting the wall properties, the absorption coefficient in combination with the shape of the moisture retention curve (MRC) were found to be most critical for the frost response behavior. Therefore, these variables, and the depression of dewpoint coupled with the shape of the MRC, were used in the definition of the clustering scheme in Figure 19. It shows the creation of three reliable clusters, where similar frost response can be found among brick types with a clear distinction in brick properties. In a practical application, a low absorptive brickwork should receive additional property measurements to reduce the uncertainty in risk assessment, especially for absorption coefficients close to zero.

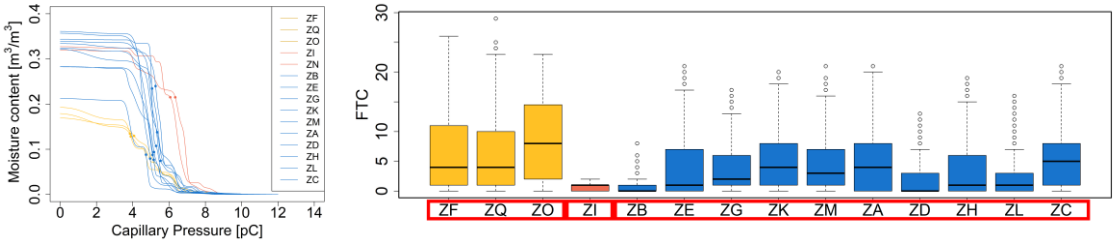

Figure 19: Left: Clustering based on the shape of the MRC Right: Clustering analysis frost degradation

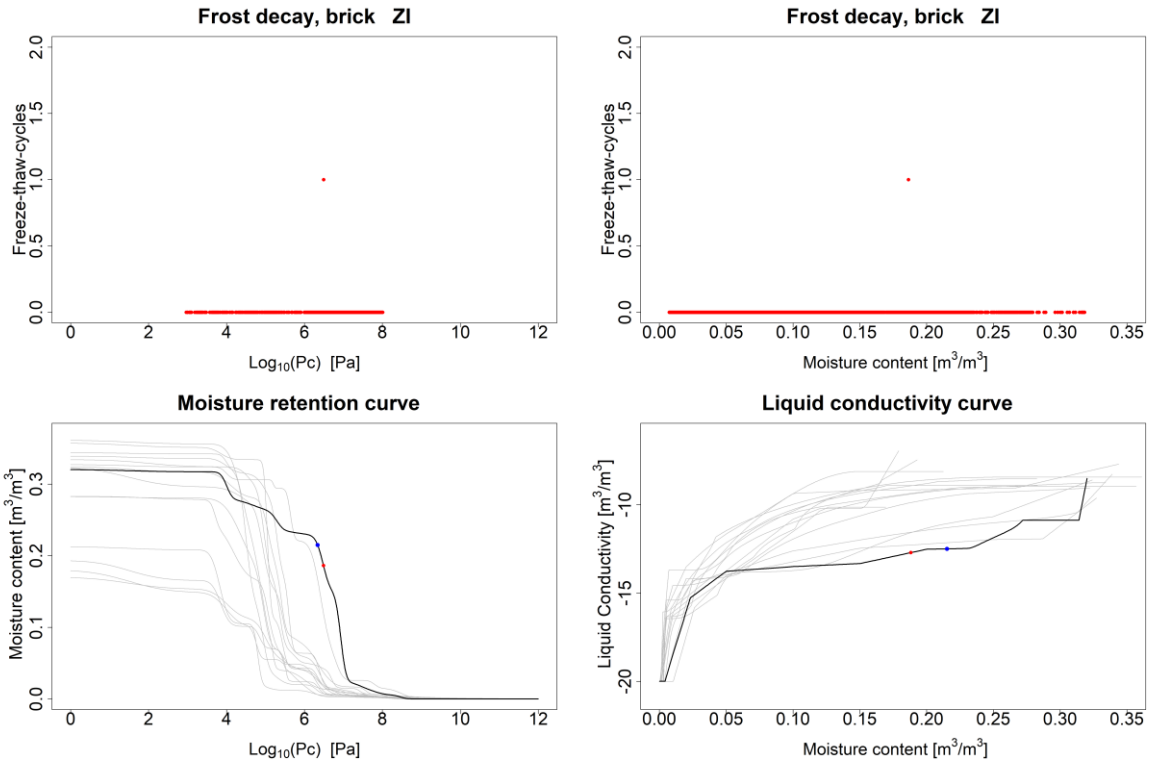

Figure 20: Top: Occurrence of FTC event as a function of capillary pressure and moisture content for a 200 mm wall of brick type ZI. Bottom: occurrence of FTC event plotted on the moisture retention and liquid conductivity curve for ZI

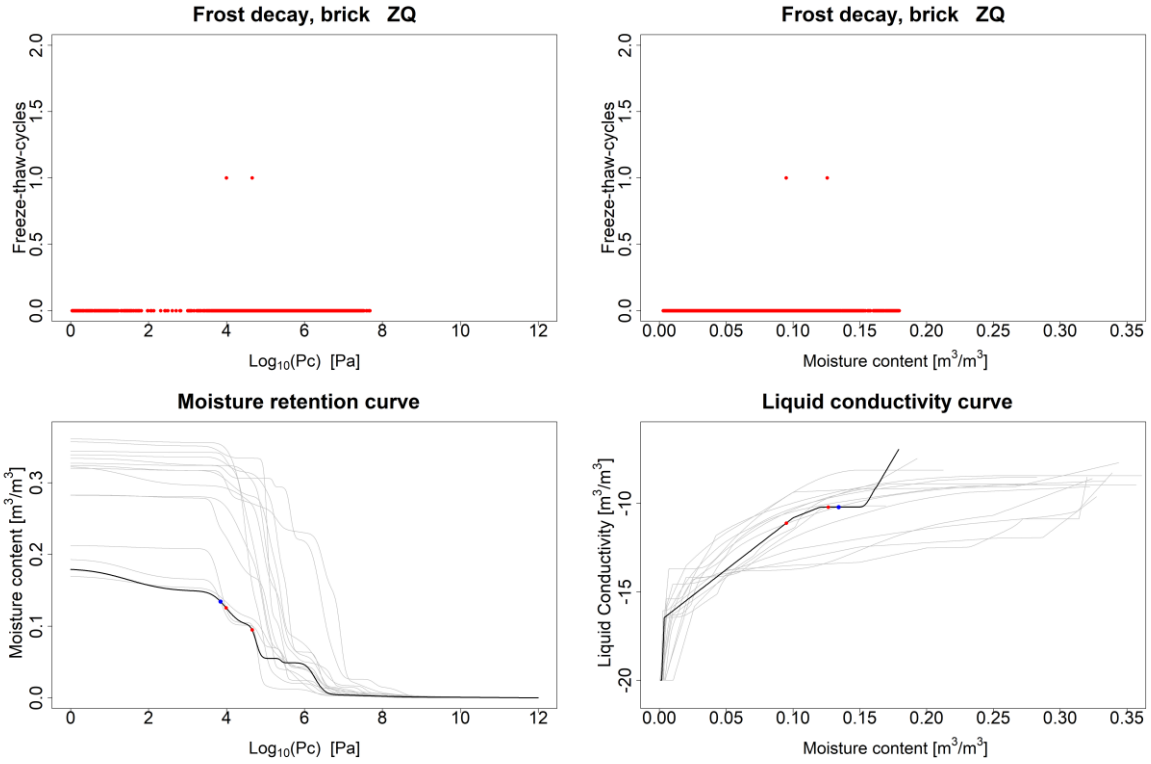

Figure 21: Top: Occurrence of FTC event as a function of capillary pressure and moisture content for a 200 mm wall of brick type ZQ. Bottom: occurrence of FTC event plotted on the moisture retention and liquid conductivity curve for ZQ

Stage 3: Overall clustering scheme based on Binary Poisson distribution trees

In the final part of this study, an overall clustering methodology for the three different decay criteria is proposed. Similarities among the individual decision trees for the degradation criteria were gathered, summarized, and compared to the clustering scheme of Zhao (2012). The conclusion was drawn in an overall classification tree in Figure 22. For all 3 degradation criteria, the absorption coefficient of the brick was most significant after the wall related properties. In reference to the clustering by Zhao, two more clusters were added to ensure adequate homogeneity in response behavior. The obtained overall clustering scheme includes a comprehensive summary regarding the risk related response behavior and the physical description for the clusters. The descriptions were approached in a similar manner as Zhao (2012), where the brick types were evaluated based on their raw material, physical appearance, and historical background.

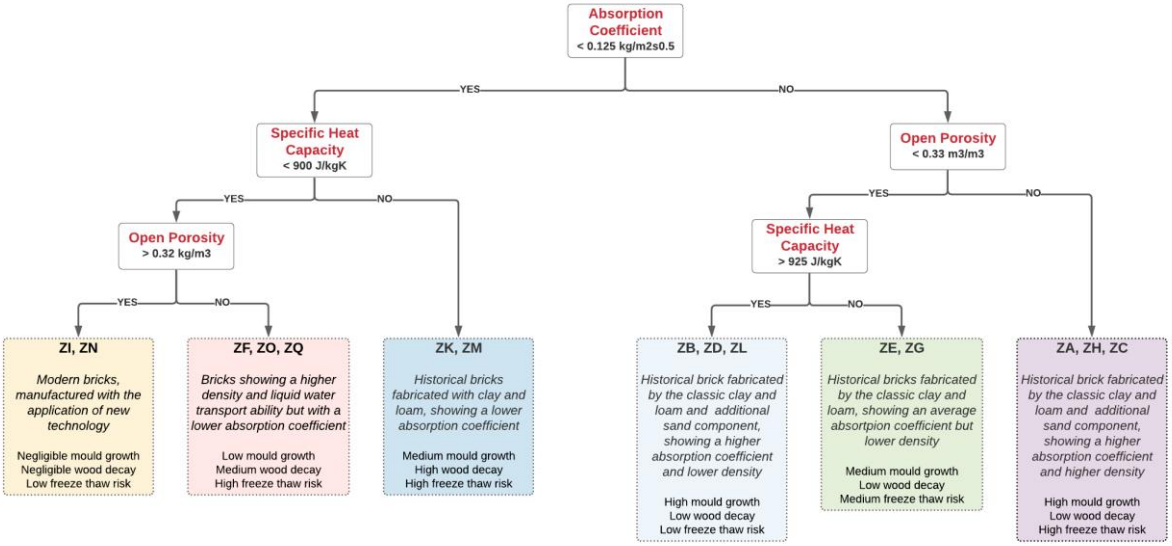

Figure 22: Overall clustering decision tree with the established clustering scheme for 15 bricks

The degradation results were clustered accordingly and visualized in Figure 23. With the developed clustering analysis and the homogeneity in response behavior and brick properties, 6 different clusters were obtained. Compared to the clustering scheme of Zhao (2012), smaller clusters were generated. Due to the smaller number of cluster elements, calculating a generic material to represent the cluster seemed ineffective. It seems more appropriate to compare a specific brickwork from in-situ renovation project with the single bricks within the assigned cluster. Note that due to the adoption of a single climate environment in the sampled cases i.e., Essen, a change in climate environment and geographical location could lead to a different clustering scheme. This is mainly because the infiltration depth of the waterfront depends on the duration and intensity of the rainfall. This study provides an overall methodology, but this should be applied for different locations and applications in future work to assess the robustness of the results.

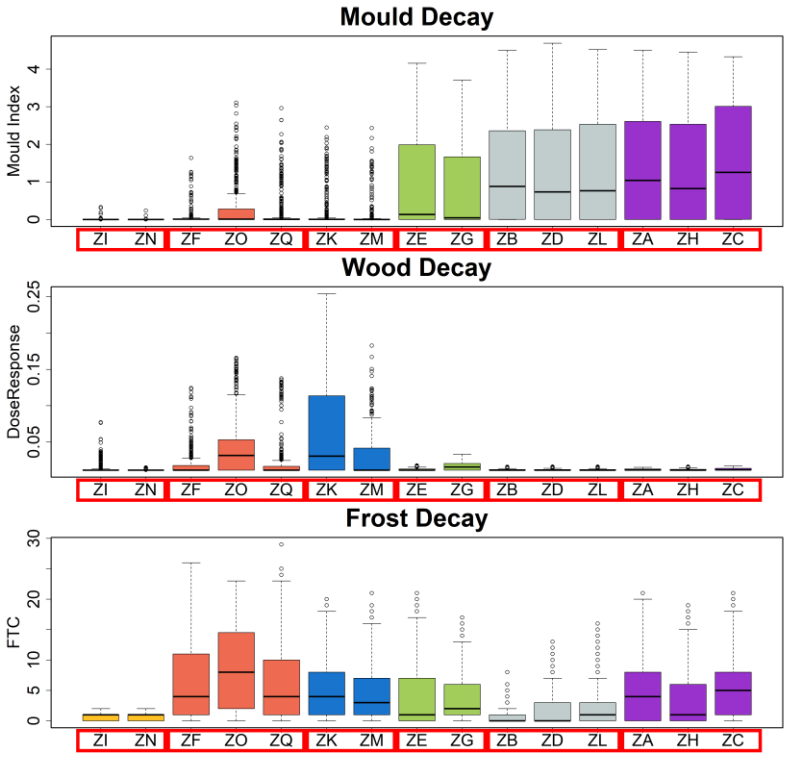

Figure 23: Overall clustering scheme of degradation profiles for: Mould decay below, Wood decay in the top left corner and Frost decay in the top right corner

Discussion

Retrofit applications can benefit from generalized guidelines and material schemes by reducing the need for extensive property measurements and computational time in risk assessments. With basic information on the brickwork (e.g., historical, loam and clay based), accompanied with additional information about the existing damage, it seems possible to use this flow chart to gain more insight in material characteristics and associated degradation risks. This study shows that the overall material flow chart can be developed based on the combination of similarities in response behavior and similarities in material properties.

However, a first caveat for the developed methodology was already made concerning the climate variables. In this study only the climate of one geographical location was used i.e., Essen. Given that the results showed a significant impact from the wind driven rain exposure, one should consider different climate locations as well as different test reference years. The climate defines the severity, duration, and numbers of rainfall events and has a direct impact on the liquid water penetration depth and the moisture content and distribution in the construction.

Secondly, the different numerical prediction models for degradation and performances are highly debated among researchers. Still many questions remain with respect to the wood decay criteria as well as the determination of frost risks. Degradation mapping and field testing on a larger scale could provide a more detailed criterion for both decay mechanisms. In addition, for wood rot assessment, the one-dimensional abstracting of the wooden beam head and the constant load bearing support should be studied in more detail for a precise risk assessment. In this study the interface resistance between the wooden beam and the brickwork was neglected but the study acknowledges that the interface as well as the load bearing length could have a significant impact on the distribution of moisture in the brickwork (Zhou et al, 2020; Gutland et al, 2021). A more precise assessment of the impact of various levels of moisture sources on the growth and initiation of wood decaying organisms could benefit the building research in a great way, especially when different wood types are to be tested.

The wide variety of brick types found in practice was represented by 23 typical bricks by Zhao (2012). Due to the limitation of information, the number was reduced to 15 bricks in this study. The latter still includes some historical brick types as well as bricks constructed with newly developed applications and technology. However, it can be questioned how representative this is for the complete range of brickwork in different countries.

Furthermore, the number of clusters was fixed on an arbitrary chosen number of 4 in Zhao (2012) and set to 6 in this study. It could be beneficial to increase or decrease the number of clusters when for example, the climate is changed drastically and the risk on an individual degradation criterion becomes negligible or rather dominant. Next to that, the small number of bricks in the current cluster highlights the need for additional information on historical bricks to assess the aptitude of the current approach. Even more, the same approach developed in this study could help provide a similar clustering overview for other building materials as well, rendering the application potential for both renovation as well as new construction even larger.

Conclusion

The aim of this study was twofold. In the first objective, the state-of-the-art clustering analysis by Zhao (2012) was evaluated. The results in this paper showed that the method did generate a reliable clustering scheme and was able to determine generic materials. However, this can only be applied when solely focusing the physical material properties. The severity of degradation and response behavior of materials was excluded. The existing approach and assumptions cause significant performance differences within a cluster and leads to incorrect predictions, which in turn reduces the reliability and application potential for practice.

The second objective was to propose a new clustering methodology with the inclusion of the response behavior for three performance criteria. Sensitivity analyses were used to determine the relation between homogeneity in response behavior and specific material properties. The results showed the dominant impact from the rain exposure coefficient for all criteria. The rain exposure determines the liquid water volume projected onto the exterior surface and thereby defines the moisture source for degradation organisms and decay processes. The response behavior for each performance criterion was defined based on the simulation results of different sample sets.

For mould decay, the absorption coefficient showed to have the most significant impact and a critical threshold at A_w = 0.1278 $kg/m^2s^{0.5}$ was established. This threshold divides the degradation profiles into two clusters, as it defines whether the waterfront reached the inner surface or whether the moisture redistributes across the masonry instead. In addition, the absorption coefficient defines the liquid transport and drying rate through the brickwork and thereby defines the relative humidity reached at the interior surface. The critical capillary pressure for mould was evaluated considering the shape of the moisture retention curve.

Homogeneity in response behavior for wood degradation was established with a threshold for absorption coefficient as well. Limited redistribution of moisture towards the interior plaster, coupled with limited drying towards the exterior surface induced high moisture contents in the beam head increasing the risk for wood rot. The A_w value of 0.14 $kg/m^2s^{0.5}$ was found crucial for development of reliable clusters. In addition, the location of the initiation moisture content in relation to the critical moisture content, defined the frequency of daily dose for wood rot.

For frost degradation, the response behavior was not only defined by the absorption coefficient. In the adopted freeze-thaw-cycles calculation model, the link between the absorption coefficient and the shape of the moisture retention curve defined homogeneity in freeze-thaw damage in relation to the material properties. The shape of the moisture retention curve has a large impact on the depression of dewpoint and on the freezing temperature required to induce frost damage.

Based on the analysis of clustering schemes, classification trees for damage criteria, and the information from Zhao regarding brick properties, it was possible to create an easy-to-handle flow chart to help the construction industry. The scheme is applicable for climates like Essen and several degradation criteria and can be adjusted for other climates and building materials.

Acknowledgement

This research was conducted to obtain the degree of *Master of Science in Engineering: Architecture (Architectural Design and Construction Techniques)*. The authors appreciate the advice and support contributed from the Ghent University in particular the building physics department.

Declaration of Conflicting Interests

The author(s) declared no potential conflicts of interest with respect to the research, authorship and/or publication of this article.

References

Andreas N. and Grunewald J. (2006) Delphin 5 User Manual and Program Reference.

ASHREA 160 (2009) Criteria for moisture-control design analysis in buildings. American Society of Heating, Refrigerating and Air Conditioning Engineers, Atlanta, US.

Brischke C. and Meyer-Veltrup L. (2016) Modelling timber decay caused by brown rot fungi. *Mater. Struct.* 49: 3281-3291. DOI: 10.1617/s11527-015-0719-y.

Brischke C. and Rapp A. O. (2008) Dose–response relationships between wood moisture content, wood temperature and fungal decay determined for 23 European field test sites. *Wood Sci Technol.* 42: 507. DOI: 10.1007/s00226-008-0191-8.

Brischke C. ,Welzbacher C., Meyer L., Bornemann T., Larsonn-Brelid P., Pilgård A., Frühwald E., Westin M., Rapp A., Thelandersson S. and Jermer J. (2011) Service life prediction of wooden components – Part 3: Approaching a comprehensive test methodology Approaching a comprehensive test methodology. In *Proceedings, IRG annual meeting Queenstown*, New Zealand, 8-12 International research group on wood protection. IRG/WP/11-20464.

Calle K. (2020) *Renovation of historical facades : the rescue or the kiss of death?* PhD thesis, Universiteit Gent. Faculteit Ingenieurswetenschappen en Architectuur, Belgium.

Calle K., Van Den Bossche N. (2021) Sensitivity analysis of the hygrothermal behaviour of homogeneous masonry constructions: Interior insulation, rainwater infiltration and hydrophobic treatment. *J. Build. Phys.* 44(6):510-538. DOI: 10.1177/17442591211009937

Campbell J. W. (2016) *Baksteen: geschiedenis, architectuur, technieken*. Nederland, Bossum: Thoth.

Carmeliet J., Hens H., Roels S., Adan O., Brocken H., Cerny R., Pavlik Z., Hall C., Kumaran K. and Pel L. (2004) Determination of the Liquid Water Diffusivity from Transient Moisture Transfer Experiments. J. *Build. Phys*. 27(4): 277–305. DOI: 10.1177/1097196304042324.

Everit B.S. and Hands S. (1987) A monte Carlo study of the recovery of cluster structure in binary data by hierarchical clustering techniques. *Multivariate Behav Res* 22: 235-243. DOI: 10.1207/s15327906mbr2202_6.

Everit B.S., Landau S., Leese M. and Stahl D. (2011) *Cluster analysis (5th edition).* West Sussex: John Wiley & Sons., Ltd. DOI: 10.1002/9780470977811.

Fagerlund G. (1975) Critical degrees of saturation at freezing of porous and brittle materials. *Conf. Durab. Concr*. 17:13-65. ACI STP, Atl.

Grunewald J., Häupl P. and Bomberg M. (2003) Towards an Engineering Model of Material Characteristics for Input to Ham Transport Simulations - Part 1: An Approach. *J. Build. Phys.* 26(4). DOI: 10.1177/1097196303026004002.

Gutland M., Bucking S., Santana Quintero M. (2021) A methodology for hygrothermal modelling of imperfect masonry interfaces. *J. Build. Phys.* 44(6) 485-509 DOI: 10.1177/1744259121989388

Hagentoft C. (2013) International Energy Agency (IEA), Annex 55 Reliability of Energy Efficient Building Retrofitting - Probability Assessment of Performance & Cost (RAP-RETRO). *Energy Conserv. Build. Community Syst.*, pp. 1–9. DOI: 10.1016/j.enbuild.2017.09.007.

Hamby D.M. (1994) A Review of Techniques for Parameter Sensitivity Analysis of Environmental Models. *Environ. Monit. Assess.* 32(32): 135–154. DOI: 10.1007/BF00547132.

Hukka A. and Viitanen H. (1999) A mathematical model of mould growth on wooden material. *Wood Sci. Technol.* 33(6): 475–485. DOI: 10.1007/s002260050131.

Kehl D. (2013) *Feuchtetechnische Bemessung von Holzkonstruktionen nach WTA.*

Kržišnik D., Brischke C., Lesar B., Thaler N. and Humar M. (2019) Performance of wood in the Franja partisan hospital. *Wood Material Science & Engineering*. 14(1): 24-32. DOI: 10.1080/17480272.2018.1438512.

Leissner J. and Killian R. (2014) *Built cultural heritage in times of climate change.* Brussel/Holzkirchen

Le Noir L. (2017) *Materialen en technieken in historische meselwerkconstructies tussen 1830 en 1945.* Master Thesis, University of Ghent, Belgium.

Mensinga P., Straube P. and Schumacher C (2010) Assessing the freeze-thaw resistance of clay brick for interior insulation retrofit projects. *Proc. Performances Envel.* Whole Build. XI, pp. 1-8

Mosoarca M., Keller A.I., Petrus C. and Racolta A. (2018) Failure analysis of historical buildings due to climate change. *Engineering Failure Analysis* 82(suppl C): 666-680. DOI: 10.1016/j.engfailanal.2017.06.013.

Ojanen T., Peuhkuri R., Viitanen H., Lädesmäki K., Vinha J., Salminen K. (2011) Classification of material sensitivity – new approach for mould growth modeling: *9th Nordic symposium on building physics* 2: 867-874.

Ojanen T., Viitanen H., Peukhuri K., Lädesmäki K., Vinha J., Salminen K. (2010) Mold growth modelling of building structures using sensitivity classes of materials. *Proceedings Build. XI*, Florida

Peirs G. (2005) *La brique, Fabrication et traditions constructives*. Paris, France: Eyrolles.

Peirs G. (1979) *Uit klei gebouwd: baksteenarchitectuur van 1200 tot 1940*. Tielt, Belgium: Lannoo.

Plagge R., Scheffler G., Meissner F., Häupl P., Fitz C., Lengfeld K., Krus M., Künzel H. and Klaus S. MASEA. (2004) Material Property Database of Old and New Building Materials for Software Tools in Building Constructions. *Proccedings of the 12th Symposium on Building Physics.* pp. 363-368. Dresden.

Rothea J. and Hoffman H. (1956) *Het bouwen met baksteen en dakpannen in Europa*. Paris, France: Fédération des Fabricants de Tuilles et de Briques

Scheffler G.A. (2008) *Validation of Hygrothermal Material Modelling Under Consideration of the Hysteresis of Moisture Storage*, PhD Thesis, University of Dresden, Germany.

Stenvert R. (2012) *Biografie van de baksteen, 1850-2000*. Zwolle, Nederland: WBooks.

Stenvert R. and Van Tussenbroek G. (2007) *Inleiding in de bouwhistorie. Opmeten en onderzoeken van oude gebouwen*. Utrecht, Nederland: Stichting Matrijs.

Vandemeulebroucke I., Calle K., Caluwaerts S., De Kock T. and Van Den Bossche, N. (2019) Does historic construction suffer or benefit from the urban heat island effect in Ghent and global warning across Europe? *Can. J. Civil Engin.* 46:1032-1042. DOI: 10.1139/cjce-2018-0594.

Vandemeulebroucke I., Defo M., Lacasse M.A., Caluwaerts S. and Van Den Bossche, N. (2021) Canadian initial-condition climate ensemble: Hygrothermal simulation on wood-stud and retrofitted historical masonry. *Build Environm*. 187. DOI: 10.1016/jbuildenv.2020.107318.

Vanpachtenbeke M. (2019) *Timber Frame Walls with Brick Veneer Cladding : Reliability to Fungal Decay*. PhD Thesis, KU Leuven. Faculty of Engineering Science; Ghent University. Faculty of Bioscience Engineering, Belgium.

Vereecken E. and Roels S. (2012) Review of mould prediction models and their influence on mould risk evaluation. *Build. Environ.* 55: 296-310. DOI: 10.1016/j.buildenv.2011.11.003.

Vereecken E. and Roels S. (2019) Wooden beam ends in combination with interior insulation: An experiment study on the impact of convective moisture transport. *Build. Environ.* 148(no. October 2018): 524-534. DOI: 10.1016/j.buildenv.2018.10.060.

Vereecken E. and Roels S. (2013) Hygric performance of a massive masonry wall: How do the mortar joints influence the moisture flux? *Constr. and Build. Components* 41: 697-707

Viitanen H. et al. (2011) Moisture and bio-deterioration risk of building materials and structures. *J. Build. Phys.* 33(3): 201–224. DOI:10.5772/21184.

Viitanen J. and Ojanen T. (2007) Improved model to predict mold growth in building materials. *Proceedings of the 10th Thermal Performance of the Exterior Envelopes of Whole Buildings Conference ASHRAE*.

Viles H.A. (2002) Implications of future climate change for stone deterioration. *Geological Society, London, Special Publications,* 205(1): 407-418. DOI: 10.1144/gsl.Sp.2002.205.01.29.

Zhao J. (2012) Development of a Novel Statistical Method and Procedure for Material Characterization and a Probabilistic Approach to Assessing the Hygrothermal Performance of Building Enclosure Assemblies. PhD Thesis, University of Syracuse. *Mech. Aerosp. Eng. - Diss.* 72. https://surface.syr.edu/mae_etd/72.

Zhao J., Plagge R., Ramos N.M.M., Simões M.L. and Grunewald J. (2015) Application of clustering technique for definition of generic objects in a material database. *J. Build. Phys.* 39: 12-146. DOI: 10.1177/1744259115588013.

Zhou X., Carmeliet J. and Derome, D. (2020) Assessment of risk of freeze-thaw damage in internally insulated masonry in a changing climate. *Build Environ.* 175 DOI: 10.1016/j.buildenv.2020.106773.

Zhou X., Desmarais G., Vontobel P., Carmeliet J., Derome D. (2020) Masonry brick-cement mortar interface resistance to water transport determined with neutrion radiography and numerical modeling. *J. Build. Phys.* 44(3): 251-271 DOI: 10.1177/1744259120908967